(Preprint) AAS 25-709

CISLUNAR DOMAIN MULTI-TARGET SEARCH AND ESTIMATION STRATEGIES AFTER LONG SENSOR SHUTOFFS*

Ishan P. Paranjape† and Suman Chakravorty‡

In this work, we extend a method for minimal-assumption probabilistic initial orbit determination (IOD) and orbit determination (OD) to track multiple objects in cislunar space. This IOD framework involves kinematically fitting polynomials through bootstrapped series of data which provide a full-position estimate. Then, an association is performed in which an observation is associated to a target estimate based on the Bayesian likelihood function. Once associations are made using data association algorithms such as the Munkres algorithm, a nonlinear filtering framework such as the Particle Gaussian Mixture (PGM) Filter is used to reduce the covariance of the target estimates over time. We primarily focus on target search and estimation methods after long sensor shutoffs, and describe the utility of autonomous search and recovery (ASR) in the process. Our combined framework allows us to generate several initial state estimates and make data associations to distinguish and track multiple targets in cislunar space.

INTRODUCTION

The extension of space situational awareness (SSA) capabilities into cislunar space is a key objective of the National Cislunar Science and Technology Strategy. Specifically, there exists a need to identify and detect several colliding objects and/or potentially dangerous spacecraft operations to ensure safe operation of spacecraft within this domain.[1] Since the volume of the cislunar domain is nearly a thousand-fold that of the volume of orbits below the geocentric (GEO) limit, and a large share of Resident Space Objects (RSOs) – also referred to more generally as targets – exist within this domain, effective cislunar target tracking becomes a crucial problem. Furthermore, with the rise of lunar missions such as China's Chang'e-5, India's Chandrayaan, and Firefly Aerospace's Blue Ghost Mission 1, it is even more imperative to ensure the safe operation of spacecraft and facilitate space traffic coordination efforts in the cislunar domain. One of the ways we can ensure this safe operation is by initializing and maintaining custody of multiple spacecraft and RSO orbits using initial orbit determination (IOD), associating between target observations and estimates, and orbit determination (OD).

The goal of IOD for a single target is to combine several measurements of a single RSO and then to fit a state vector through the measurements.[2] For multi-target tracking, this goal is simply extended to multiple RSOs. One of the most well-known methods of IOD is Gauss's Method.[3]

†Graduate Assistant - Research, Department of Aerospace Engineering, Texas A&M University, 710 Ross St., College Station, TX 77843.

‡Professor, Department of Aerospace Engineering, Texas A&M University, 710 Ross St., College Station, TX 77843.

However, more specialized IOD methods such as constrained admissible region (CAR) and probabilistic admissible region (PAR) persist throughout literature.[4–7] *Mishra et. al. 2024* utilize PAR to generate initial estimates of a target within regimes up to geosynchronous orbit (GEO), the point up to where the effects of the two-body problem are valid. More specifically, their IOD framework involves postulating statistics about four of the six major orbital elements as *a priori* information and generating multiple observations of the target state using those statistics.[8] Along with two angular measurements, an initial state estimate is formulated. *Bolden et. al. 2022* and *Griggs et. al. 2023* utilize PAR to generate a similar set of initial orbit estimates.[9,10] Since traditional orbital elements cannot be used effectively in the cislunar domain, where effects of the three-body problem dominate, the authors rely upon postulated statistics of the range utilizing light intensity curves generated by *Hejduk 2013*, sensor movement constraints for angular rates, and the singular constant of integration (Jacobi's constant) produced by the equations of motion of the circular-restricted three-body problem (CR3BP).[11] *Mishra et. al. 2024*, *Bolden et. al. 2024*, and *Griggs et. al. 2023* all utilize the same OD framework: the Particle Gaussian Mixture (PGM) Filter.[8,12]

While *Bolden et. al. 2022* and *Griggs et. al. 2023* provide an effective method for IOD with PAR by utilizing realistic constraints, their method relies on postulating several statistics, resulting in lots of *a priori* assumptions. Gauss's method for orbit determination is a popular benchmark for IOD due to its limited use of assumptions and the simplicity associated with obtaining an initial state estimate of an RSO up to the GEO regime by using three consecutive short-arc measurements. Although we cannot apply Gauss's method to the cislunar domain, we are able to perform probabilistic IOD and target tracking with less initial information and fewer postulated statistics.

In this work, we focus on multiple-object tracking (MOT) scenarios. Here, we are no longer able to utilize the assumption that all measurements came from the same RSO. Instead, optical sensors will observe multiple targets in a single observation, requiring associations between observations and cataloged objects. When a significant number of RSOs exist, there exists combinatorial growth in the number of "hard" observation-to-observation (obs-obs) association possibilities.[13,14] Luckily, due to the expanse of the cislunar domain relative to regimes up to geosynchronous orbit (GEO), relatively far fewer targets exist within this domain, and data association steps do not necessarily become far too computationally taxing. As a result, we are able to add a data association step to our IOD/OD framework.

In this work, we seek to extend the combined IOD/OD framework introduced in *Paranjape and Chakravorty 2025* to MOT scenarios in the cislunar domain.[15] We continue to use minimal assumptions through our IOD framework of kinematically fitting polynomials through our observations and using the PGM framework for target tracking, adding an association step prior to the update step. The remainder of this paper is organized as follows. First, we introduce our combined IOD and OD framework consisting of a nonlinear dynamics model and a nonlinear measurement model. We include a discussion about our multi-target tracking framework and outline a method utilized for associating observations with estimates. Then, we present some multi-target tracking scenarios for a chaotic orbit with two targets, particularly after sufficiently long sensor-shutoffs, varying only the initial separation distance between the two targets. We finally discuss the topic of autonomous search and recovery in the context of obtaining measurements after long periods of sensor shutoffs.

FUNDAMENTALS OF CISLUNAR TARGET TRACKING

Effective multi-target tracking in the cislunar domain requires an IOD method for generating initial state estimates and an OD method for continuous tracking and maintaining custody of multiple

RSOs. In near-Earth regimes (i.e. LEO, GEO), targets move quickly relative to the Earth's rotation due to the force of gravitational attraction induced by the Earth to these RSOs, allowing optical sensors only a brief glimpse of RSO trajectories. The MOT problem is compounded in this regime by the fact that there are overwhelmingly more targets within the GEO limit than outside of it.[16] In that regard, the cislunar regime offers us some distinct advantages for MOT.

Due to the vastness of the cislunar domain, an RSO may appear in the line of sight (or field of view) of an observer – typically an optical sensor or radar observatory – for 10-20 hours at a time, resulting in our ability to make several consecutive observations. The relatively small number of targets in the cislunar domain allows us to better distinguish targets without facing issues with combinatorial growth in the number of associations. It is also important to note that those hours-long passes in cislunar space are much longer than the minutes-long passes of RSOs up to the GEO limit. This fact allows us to piece a state vector through several consecutive observations to effectively estimate the state of a target at some point along the first pass of observations. Before we describe this IOD method in greater detail, we shall outline the dynamics and measurement models we shall use for our combined IOD/OD framework.

Dynamics Model

Beyond the GEO regime, effects of larger gravitational bodies such as the Moon and the Sun become apparent, and the use of Keplerian orbital elements start to become obsolete, as orbits are no longer continuously conic in nature. Nevertheless, several dynamics models exist in celestial mechanics for the cislunar regime, the most popular of which is the circular-restricted three-body problem (CR3BP).[17] CR3BP dynamics are expressed in a synodic reference frame, whose center is located at the center of mass (or barycenter) of the two largest orbiting bodies. These larger bodies rotate in a circular motion about their barycenter. Due to the mass of the Earth relative to its Moon, the system barycenter lies within the Earth itself. The RSO is treated as a third body with negligible mass relative to the other two bodies. The equations of motion of the RSO with respect to this barycentric frame are given below.

$$\ddot{x} = x + 2\dot{y} - \frac{(1-\mu)(x+\mu)}{r_1^3} - \frac{\mu x - \mu(1-\mu)}{r_2^3} \tag{1a}$$

$$\ddot{y} = y - 2\dot{x} - \frac{(1-\mu)y}{r_1^3} - \frac{\mu y}{r_2^3} \tag{1b}$$

$$\ddot{z} = \frac{(1-\mu)z}{r_1^3} - \frac{\mu z}{r_2^3} \tag{1c}$$

In the equations above, x and y define the orbital plane of the larger bodies 1 and 2, r_1 and r_2 define the distance between the target and the centers of mass of bodies 1 and 2, respectively. μ is a constant mass parameter that defines the weights of the two major bodies relative to each other. All mass, time, and distance quantities are expressed in non-dimensional units.[17]

Measurement Model

A traditional radar or optical sensor provides measurements of azimuth and elevation. Range may also be obtained by calculating round-trip return time and other methods. Due to the vastness of cislunar space, however, range measurements are not always reliable or accurate, whereas angular

measurements are much more reliable. To mitigate this issue, we assume that our measurement model's noise statistics for range encompass a sufficiently large fraction of the true range value, while the angular noise statistics are kept low due to the high fidelity of current optical and radar sensors. The following set of equations relate range, azimuth, and elevation with state coordinate components in an observer-centered topocentric reference frame. The conversion of range, azimuth, and elevation information to topocentric position information involves simple algebraic manipulations. From Eqs. 2, it is also possible to get values for the topocentric x, y, and z coordinates, yielding a full-position estimate.

$$R = \sqrt{x^2 + y^2 + z^2} \tag{2a}$$

$$AZ = tan^{-1}(\frac{y}{x}) \tag{2b}$$

$$EL = \frac{\pi}{2} - cos^{-1}(\frac{z}{\sqrt{x^2 + y^2 + z^2}}) \tag{2c}$$

Initial Orbit Determination

In our introduction, we alluded to the fact that RSOs in cislunar space stay within an observer FOV for up to 20 hours at a time. During that time period, we may obtain estimates for $x(t)$, $y(t)$, and $z(t)$ in the topocentric reference frame with a sufficient number of observations. By utilizing the curve fitting approach outlined in *Paranjape & Chakravorty 2025*, we obtain an initial state estimate for a single target expressed in particle form in Figure 2.

Briefly, this curve fitting approach involves fitting curves through topocentric x, y, and z as functions of time by manipulating Eq. 2, which provide a full-position estimate of the system, in spite of low range accuracy. If we sample from from our noise statistics a large number of measurements resulting in time-series signals of noisy data, we shall obtain several different points for $x(t)$, $y(t)$, $z(t)$, $\dot{x}(t)$, $\dot{y}(t)$, and $\dot{z}(t)$ in the topocentric frame, providing us a full-state estimate, indicated by the starred endpoints in Figure 1. When this procedure is bootstrapped over hundreds or thousands of data points, the result is a particle cloud such as that shown in Figure 2, in which each particle represents a single state estimate derived from the starred points in Figure 1.

Orbit Determination

Proper orbit determination of a highly nonlinear system coupled with a highly nonlinear measurement model requires a sophisticated filter, specifically one which utilizes a Gaussian Mixture Model (GMM) for *a priori* estimates.

For our OD framework, we shall continue to use the recursive Particle Gaussian Mixture (PGM) filter developed by *Raihan & Chakravorty 2018* and applied by *Bolden et. al. 2022*, *Griggs et. al. 2023*, and *Mishra et. al. 2023*.[9,10,12,14] Unlike traditional particle filters, the PGM filter has a clustering step. The clusters (represented as GMM components) each have an associated weight, mean vector, and covariance matrix, which altogether formulate an *a priori* estimate. We update each cluster's mean vectors and covariance matrices with a Kalman update, and the *a priori* weights using the Bayesian likelihood function, treating each *a priori* GMM component as an ensemble of particles. The resampling step at the next time step will use Markov Chain Monte Carlo (MCMC) sampling to draw from this posterior distribution. The Particle Gaussian Mixture algorithm is detailed in Algorithm 1, copied from *Raihan & Chakravorty 2018*.

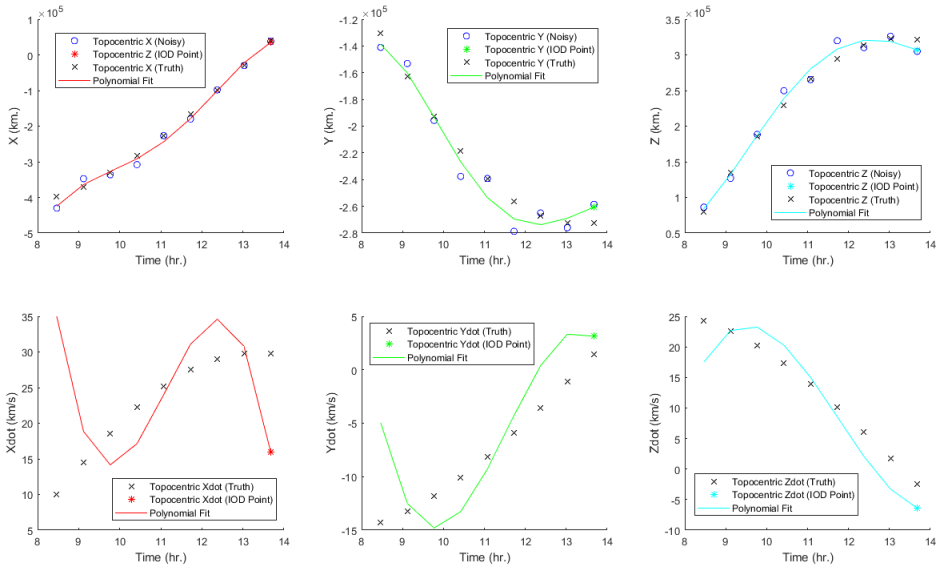

Figure 1: Polynomial fitting over half (50%) of an RSO's pass. Fourth order polynomials as functions of t are fitted through topocentric x, y, and z data. When their temporal derivatives are taken, an estimate for the IOD is formed at the last timestep in these plots (indicated by a star symbol). Mutiple sets of measurements are bootstrapped to accomplish a good initial state estimate.

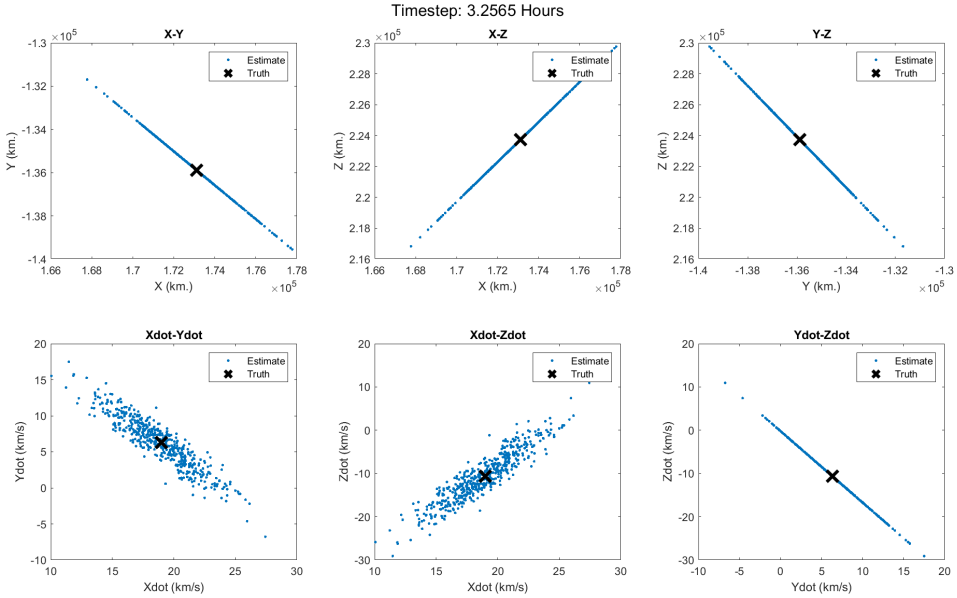

Figure 2: The final result of our IOD framework is encapsulated within this particle cloud (in blue), within which the target's true state (given as a black cross) lies. This is the result of fitting several signals of bootstrapped time-series data derived from noise statistics.

Algorithm 1 Particle Gaussian Mixture Filter Algorithm

- Given $\pi_0(x) = \sum_{i=1}^{M(0)} \omega_i(0) p_g(x; \mu_i(0), P_i(0))$, transition density kernel $p(x'|x)$, $n = 1$.
  1. Sample N_p particles from π_{n-1} and the transition density kernel $p_n(x'|x)$ as follows:
     - Sample $X^{(i)'}$ from $\pi_{n-1}(.)$.
     - Sample $X^{(i)}$ from $p(.|X^{(i)'})$.
  2. Use a clustering algorithm $\mathcal{C}$ to cluster the set of particles $X^{(i)}$ into $M^-(n)$ Gaussian clusters with weights, mean, and covariance given by $\{\omega_i^-(n), \mu_i^-(n), P_i^-(n)\}$.
  3. Update the mixture weights and mixture means and covariances to $\{\omega_i^+(n), \mu_i^+(n), P_i^+(n)\}$, given the observation z_n, utilizing the Kalman update.
  4. $n = n + 1$. Go to Step 1.

The difference between single-object tracking and multi-target tracking is that an additional association step will need to be performed between the clustering and update steps. We outline this approach in the following subsection.

Data Association

For the data association step, we utilize the Munkres (i.e. Hungarian) algorithm.[18] The Munkres algorithm solves a cost minimization problem in which, in the context of MOT with K targets, involves associating or mapping observations to estimates or probability density functions (PDFs). Each component of the data association matrix, which we label $\mathbf{D} \in R^{K \times K}$, is computed as follows:

- From the clustering step, we are given $\{\omega_i^-(n), \mu_i^-(n), P_i^-(n)\}$ as some target j's *a priori* estimate. There are k possible observations from which to choose, denoted by the set $\{\mathbf{z}_k\}$.
- Using the law of total probability, the likelihood that observation/measurement k may be associated with the i^{th} GMM component of your estimate, $l_i(\mathbf{z}_k)$, is computed for each cluster.
- The product of the *a priori* cluster weight and the likelihood are taken for each cluster and summed. The resulting summation becomes element $\mathbf{D}_{jk}$ of the data association matrix.

The goal of the Munkres algorithm is to minimize the sum of associations such that each observation is assigned to at most one *a priori* PDF estimate. However, we wish to maximize the volume (i.e. product) of data association likelihoods in $\mathbf{D}$, as opposed to a sum, resulting in a modification of the elements of our data association matrix. A key property of logarithmic algebra is that the logarithm of a product of several numbers is the sum of the logarithm of each of those numbers. As a result, we take the logarithm of each $\mathbf{D}_{ij}$. To convert the minimization algorithm into a maximization algorithm, we simply negate each component. Our new data association then becomes $\tilde{\mathbf{D}}$, whose elements are related to the elements of $\mathbf{D}$ by the equation below:

$$\tilde{\mathbf{D}}_{ij} = -\log \mathbf{D}_{ij}. \tag{3}$$

For data associations in the proceeding section, we assume that there are at most the same number of observations as estimates.

RESULTS AND DISCUSSION

Due to large distances and smaller number of targets in cislunar space, it may be shown that, assuming you have two sufficiently spaced RSOs initially, the problem of data association in multi-target tracking becomes benign. One can easily distinguish objects in cislunar space, even after long periods of sensor shutoffs (i.e. months-long maintenance work or major, long-term technical issues with ground-based optical sensors). In this section, we focus on an orbit in which targets pass close to the L_2 Lagrange point at small velocities. This orbit is chosen due to the interesting warping pattern and cluster bifurcation of particles propagated over a long period of time from a region around this L_2 Lagrange point. Kinematic fitting through observations of both targets yields the initial state estimates given by Figure 3.

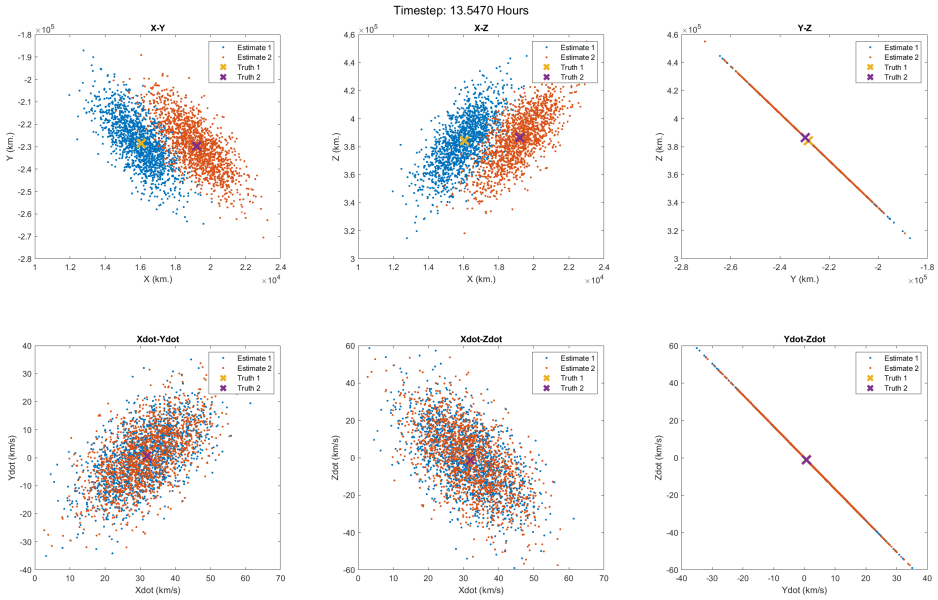

Figure 3: A particle-based representation of an initial state estimate for a set of two targets spaced 4000 km. apart initially and which will be orbiting near the L_2 Lagrange point after 48 hours at a small velocity. A polynomial is fitted through roughly 50% of the first pass for topocentric x, y, and z data, obtained algebraically from our measurement model and Eq.2. From here, our OD framework – which consists of propagation, clustering, association, and update steps – shall be used to shrink the size of our initial state estimate.

The experimental setup in Figure 3 allows us to track each target for a sufficient amount of time to properly distinguish each object, and to reduce our target uncertainty with the PGM framework during those initial 48 hours. Afterwards, both target estimates will be expected to show significant overlap in the state and/or measurement spaces. Furthermore, after the initial state estimate is obtained in Figure 3, we utilize an angles-only (i.e. azimuth and elevation) measurement model to reduce the uncertainty. For roughly 30 hours from obtaining our initial state estimate, we propagate, cluster, associate, and update as is possible to reduce the size of our particle cloud (i.e. estimate) to streaks shown in Figure 4 below. The streak patterns are indicative of the fact that we only have angular information in the observation model, resulting in long errors in the range (which are

nevertheless reduced over time).

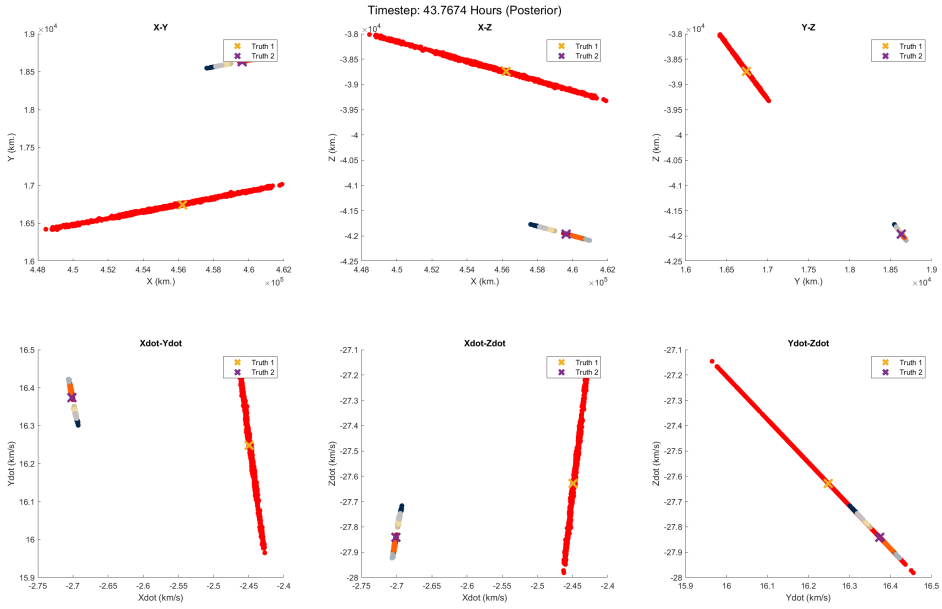

Figure 4: Iterative propagation, clustering, association, and update steps over 30 hours since obtaining an initial state estimate will give us state estimates – depicted in particle form – from which we can easily distinguish observations and targets. From this point, we shall assume a long-term sensor shutoff during which we only propagate particles each time step. Here, a reason that one target estimate is much larger than another is that the target defined by the smaller estimate had more observations (and thus more update steps) associated to it than the first target.

After these 30 hours, we introduce a roughly 20-day sensor shutoff period during which particles drawn from the posterior estimate that fused the most recent observation are propagated continuously over time for both estimates. We also increase the time cadence of the PGM filter from roughly every 40 minutes to once every 8-16 hours. Over time, the state estimates for both targets warp and ”grow” to a point at which observations would start becoming indistinguishable (i.e. observations are wrongly associated for both targets or multiple targets). An example of how both PDFs evolve up to the last time step prior to receiving an observation is shown below.

After we propagate all of the particles in both estimates shown in Figure 5 for eight more hours and cluster, we may utilize Bayes' rule and the likelihood function to compute the elements of our data association matrix. The results for our example are shown in Table 1. In order to obtain a proper data association, each element in the data association matrix is transformed using Eq. 3, but this transformation is not shown in the matrices provided within this section. From Table 1, it is clear that Observation 1 is to be associated with Target Estimate 1 and Observation 2 is to be associated with Target Estimate 2. Performing the appropriate association and update steps results in a posterior estimate shown in Figure 6.

Post-shutoff data association for initial separation distances of 4000 km. or more becomes a benign problem. However, it is also important to know the limits at which data association becomes

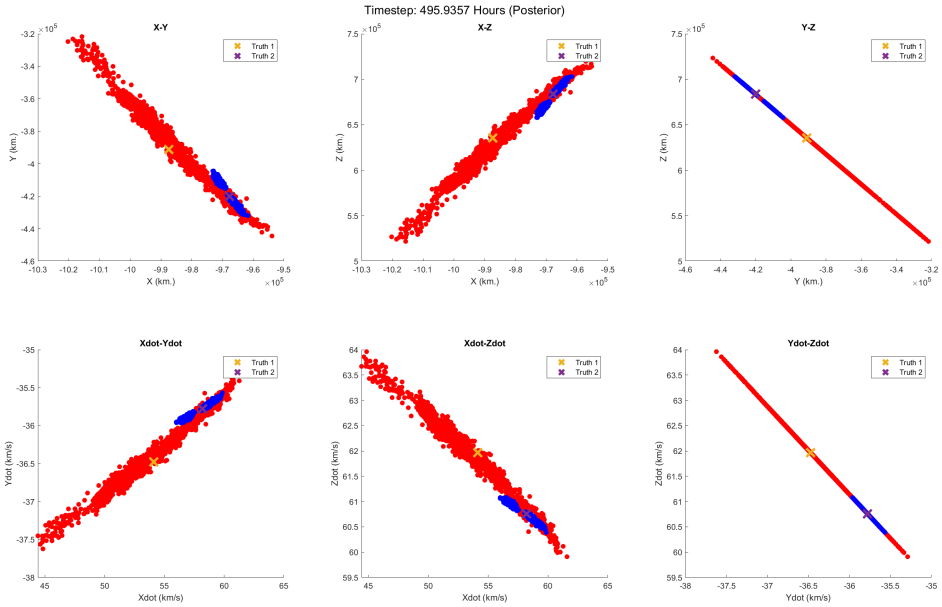

Figure 5: Starting with the particle clouds in Figure 4, propagation of both particle clouds over a period of 20 days results in nearly indistinguishable state estimates. However, the large difference in size between the estimates will allow us to more easily distinguish which observation will not be likely to be associated with the smaller initial state estimate, reducing the risk of an incorrect data association.

Observation	Target Estimate 1	Target Estimate 2
1	1.73×10^5	1.03×10^{-83}
2	4551	1.10×10^5

Table 1: Data association matrix $\mathbf{D}$ for target estimates after a sensor shut-off of 20 days.

suboptimal. To this end, we present several tabulated data association matrices $\mathbf{D}$ for initial target separation distances varying between 1000 km. to 10000 km. It becomes clear that for initial separation distances greater than roughly 1900 km., the post-shutoff data association becomes more and more benign due to the diagonal dominance of the component values. Note that for both Tables 1 and **??**, only the values for $\mathbf{D}_{ij}$ are given. To use the Hungarian algorithm, one would have to transform each value of the matrix using Eq. 3.

AUTONOMOUS SEARCH AND RECOVERY

Autonomous search and recovery (ASR) – also known as autonomous search and tracking (SAT)[19] – in the context of cislunar target tracking refers to the problem of finding targets of interest in the sky and keeping a catalog of these objects once found. ASR is particularly useful for retaining custody of targets after periods of long sensor shutoffs, as was discussed in the previous section.

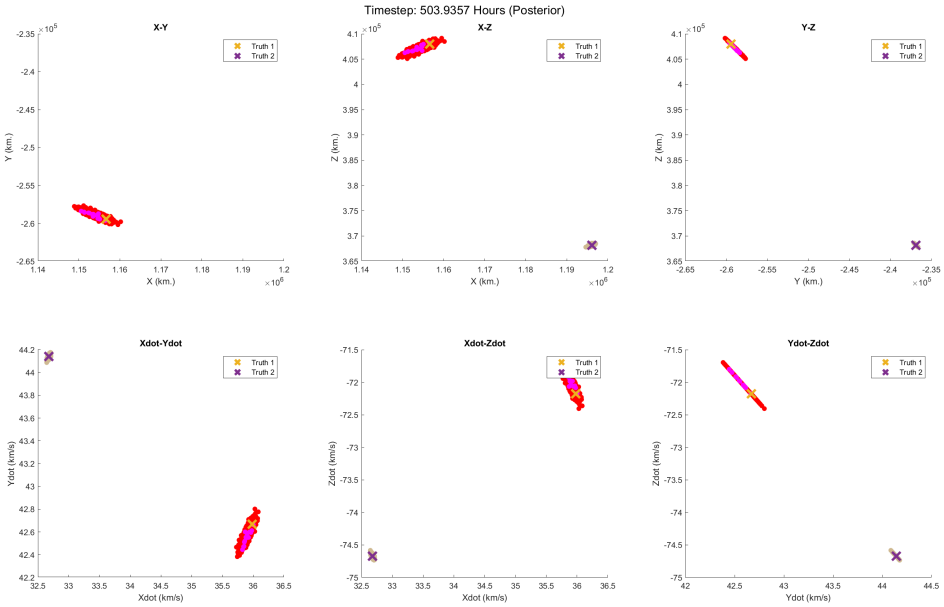

Figure 6: Association and update steps on the *a priori* estimates for both targets result in two clearly distinguishable target estimates after this sensor shutoff. From here, it becomes easy to apply our OD framework over time to maintain custody of both targets.

Although a particle representation of target estimates may suggest sufficient spacing between targets at one timestep, such as that shown in Figure 4, propagation of each particle over sufficiently long periods of time will result in a mixing of particles such as that shown in Figure 5, at which point the PDF of Target 2 is almost completely "contained" within the PDF of Target 1. A major reason we are able to distinguish between the two targets once the shutoff is over is that prior to the shutoff, Target 2's PDF has a smaller overall uncertainty due to staying in the sensor FOV longer. In the state and measurement spaces post-shutoff, this allows us to visually and logically determine that while the measurement corresponding to Target 2 may also correspond to Target 1, there is no chance that a measurement corresponding to Target 1 would correspond to Target 2's estimate.

Unfortunately, most target-tracking scenarios are not like this. However, it may be possible to retain custody of targets after long sensor shutoffs by visually examining the evolution of target estimates in the measurement space. In this section, we demonstrate the application of ASR for two target tracking scenarios which result from long sensor shutoffs.

Example 1: 9:2 Resonant Near-Rectilinear Halo Orbit

NASA's Gateway refers to the lunar space station in orbit around the Moon. The module shall serve as an outpost for astronauts of the upcoming Artemis mission. This Gateway module is placed in what is known as a 9:2 resonant near-rectilinear halo orbit (NRHO) due to the ease of transfer to other orbits in cislunar space and low orbit maintenance costs.[20,21] For our first example, we place two targets in the neighborhood of this 9:2 NRHO orbit with a separation distance of less than 1000 kilometers at the IOD step. From this point, we propagate, cluster, associate measurements, and update our state estimates for roughly 24 hours before assuming a 30-day sensor shutoff. Figures 7

(a) Initial Separation Distance: 1000 km.

Observation	Target 1	Target 2
1	3.52×10^4	5.80×10^4
2	8.25×10^3	5.36×10^5

(b) Initial Separation Distance: 1900 km.

Observation	Target 1	Target 2
1	9.30×10^4	3.23×10^4
2	2.88×10^4	4.80×10^5

(c) Initial Separation Distance: 5000 km.

Observation	Target 1	Target 2
1	1.77×10^5	0
2	1044	1.58×10^8

(d) Initial Separation Distance: 10000 km.

Observation	Target 1	Target 2
1	2.24×10^5	0
2	2.97×10^{-10}	1.02×10^8

Table 2: Data association matrices $\mathbf{D}$ after the 20-day sensor shutoffs for increasing initial separation distances. It may be observed that as the initial separation distance increases, the diagonal dominance after long sensor shutoff times tends to increase.

and 8 show our state estimates prior to and just after the sensor shutoff in the state and measurement spaces.

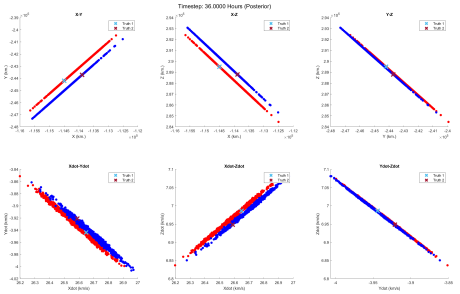

(a) Pre-shutoff target estimates in state space.

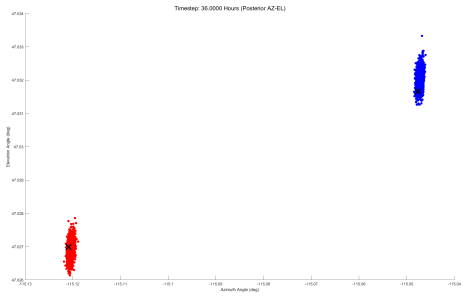

(b) Pre-shutoff target estimates in measurement space.

Figure 7: Pre-shutoff estimates for targets in the neighborhood of the 9:2 NRHO.

In reality, most realistic sensor shutoffs last between one to three weeks. We demonstrate the effect of a 30-day sensor shutoff in this example to demonstrate the evolution of our target estimates over time for some of the worst case scenarios. In Figure 7, our target estimates began as two distinguishable objects in our sensor FOV. Due to nonlinearity in dynamics, the two target estimates begin to mix together such that there exist overlaps in the state estimate between both distributions. In Figure 8, these overlaps are evident. However, in the measurement space, the two state estimates are more distinct and express a signature, which we define as a line-like shape or streak of particles in the measurement space. The overwhelming majority particles of Target 1's estimate lie along a roughly parabolic curve of roughly one-degree thickness while the particles of Target 2's estimate lie along a short, straight streak of similar thickness.

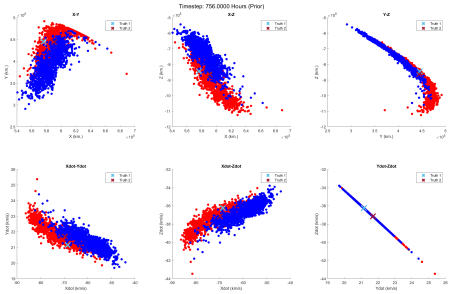

(a) Post-shutoff target estimates in state space.

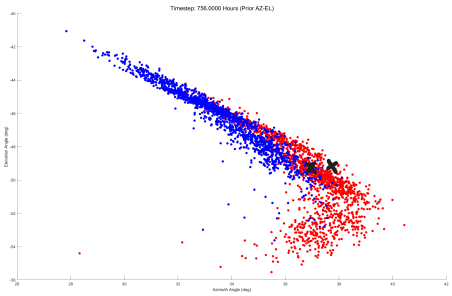

(b) Post-shutoff target estimates in measurement space.

Figure 8: Post-shutoff estimates for targets in the neighborhood of the 9:2 NRHO.

Although the uncertainty of each target estimate has grown and stretched, the signatures of both targets are narrow enough that a sensor only has to point to a certain curvy path in the sky in order to locate both targets. In this example, because targets are more visibly distinguishable, visual association is possible, after which our tracking scenario may be continued. We may also use the Munkres Algorithm to mathematically distinguish targets and state estimates.

Example 2: Chaotic Warping Past L_2 Lagrange Point

We revisit the running example in this article related to chaotic warping about the L_2 Lagrange point. In the examples shown in the previous section, we utilized our multi-target PGM framework to reduce the uncertainty of our target state over 36-48 hours. In this example, we only reduce the uncertainty of our state over a single, 24-hour length pass, but with slightly more frequent measurements. If the pre-shutoff target estimate certainties are long enough, they shall warp into spiral or tadpole-shaped PDFs after shorter (i.e. less than two weeks) sensor shutoffs. To illustrate our point, we provide pre- and post-shutoff target estimates in the state and measurement spaces in Figures 9 through 11.

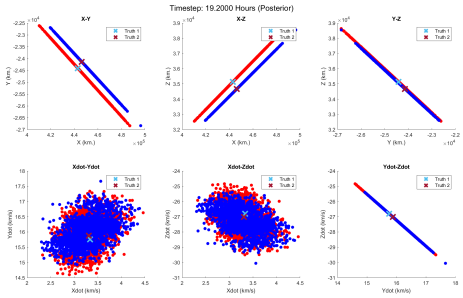

(a) Pre-shutoff target estimates in state space.

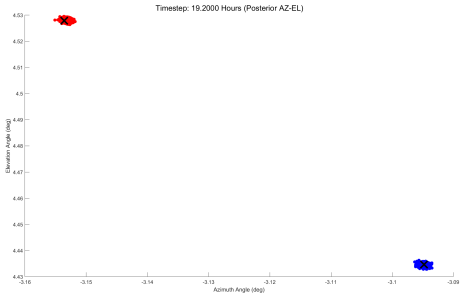

(b) Pre-shutoff target estimates in measurement space.

Figure 9: Pre-shutoff estimates for targets in the neighborhood of trajectories passing near L_2 Lagrange point.

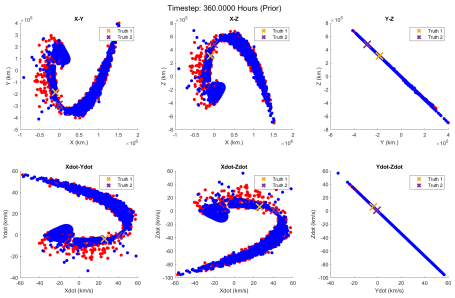

(a) Post-shutoff target estimates in state space.

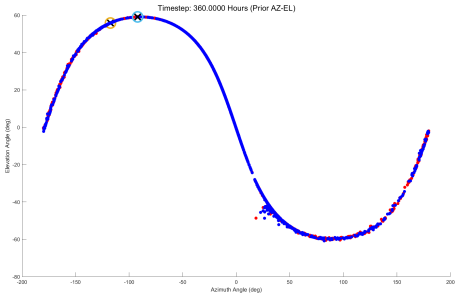

(b) Post-shutoff target estimates in measurement space.

Figure 10: Post-shutoff estimates for targets in the neighborhood of trajectories passing near L_2 Lagrange point.

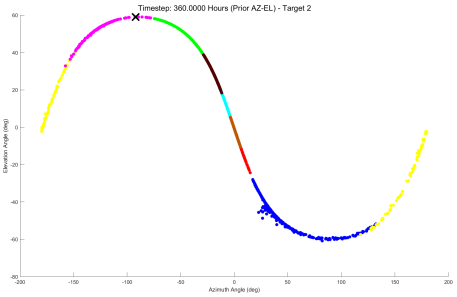

(a) Measurement space signature for the PDF describing Target 1.

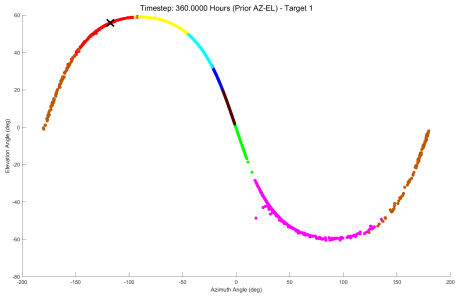

(b) Measurement space signature for the PDF describing Target 2.

Figure 11: Individual measurement signatures for the targets shown in Figure 10b, clustered by state.

Comparing Figure 10a to Figures 10b, 11a, and 11b, it is clear that although the estimate PDFs for Targets 1 and 2 warp continuously in the state space to the shape of spirals or tadpoles, the translation of each particle from Figure 10a into a measurement space yields a very narrow, almost sinusoidal curve. In other words, as the PDF in Figure 9 is propagated continuously throughout the shutoff, the state estimate, however non-Gaussian in the state space, propagates along a curve almost perfectly in the measurement space.

Two reasons for the shape of the target estimates in Figure 11 are high angles-only precision and distance from Earth. For the examples throughout the previous and current sections, we assume azimuth and elevation angle measurement errors to be additive and distributed as zero-mean Gaussian with uncertainties of 1.5 arcsec apiece. Due to the high precision of angular measurements, target estimate PDFs in the measurement space start so small and distinct (as shown in Figure 9) that they grow along a curve much faster than they grow outward; only a few particles tend to deviate from this curve.

Due to the unstable equilibrium associated with the L_2 Lagrange point, some target passing through or near such a point at even a minimal velocity will drift hundreds of thousands, even

millions, of kilometers away from the Earth. Due to the large distances within cislunar space, particles that may be widely distributed in the state space (like for Figure 10a) appear along narrow curves in the measurement space (see Figure 10b). The narrow, "linear" shape of these measurement signatures enable an observer to simply search a small, narrow region of the sky for our targets of interest, rather than trying to search the entire sky. Based on the number of observations received, it is possible to associate measurements with estimates. Although the measurement signatures in our example have considerable overlap after a roughly two-week sensor shutoff, target estimates may be resolved using the Munkres Algorithm.

CONCLUSIONS AND FUTURE WORK

In this paper, we extended the single-target IOD/OD framework introduced in *Paranjape & Chakravorty 2025*. This new combined framework involves IOD by fitting a polynomial through series of range, azimuth, and elevation angle observation data to obtain an initial state estimate for multiple targets. Then, due to the nonlinearity of cislunar dynamics and our measurements, we presented an OD framework in the form of the PGM filter, which is robust to both stable and unstable cislunar orbits. We also added an association step between the clustering and update steps, which involves using Munkres algorithm. We demonstrated the use of our IOD/OD framework on a set of orbits involving two targets passing close to the L_2 Lagrange point at small velocities, and demonstrated the effect of initial separation distances on data association ability after prolonged periods without observations. Finally, we discussed the utility of autonomous search and recovery in the context of long sensor shutoffs.

There are several improvements and extensions that we wish to make to this work. Although we have demonstrated our combined, multi-target IOD/OD framework for a system of two targets, we wish to apply more multi-object tracking scenarios proposed such as target births and possible target deaths to RSOs in cislunar space.[13,14] We also wish to explore the utility of our framework for multi-target chaser/follower target configurations such as loitering scenarios within the 9:2 resonant NRHO region.[22] We also wish to study the utility of this combined IOD/OD framework with more complex dynamics models such as the general restricted three-body problem (R3BP) or the bicircular-restricted four-body problem (BCR4BP).[23]

ACKNOWLEDGMENT

The authors of this paper are grateful to the United States Space Force (USSF) Chief Technology and Innovation Office for funding this project. Furthermore, the authors are grateful to Dr. Jill Bruer of the United States Space Force for robust technical discussions and feedback regarding this project and future improvements.

REFERENCES

[1] *National Cislunar Science Technology Strategy*. Washington, DC: National Science and Technology Council, 1st ed., 2022.

[2] R. Gooding, "A New Procedure for the Solution of the Classical Problem of Minimal Orbit Determination from Three Lines of Sight," *Celest. Mech. Dyn. Astron.*, Vol. 66, No. 4, 1997, pp. 387–423.

[3] L. Taff, "ON GAUSS'S METHOD OF ORBIT DETERMINATION," tech. rep., Massachusetts Institute of Technology Lincoln Laboratory, 06 1979.

[4] K. J. DeMars and M. K. Jah, "Probabilistic Initial Orbit Determination Using Gaussian Mixture Models," *Journal of Guidance, Control, and Dynamics*, Vol. 36, No. 5, 2013, pp. 1324–1335, 10.2514/1.59844.

[5] M. S. Tom Kelecy and M. Jah, "APPLICATION OF THE CONSTRAINED ADMISSIBLE REGION MULTIPLE HYPOTHESIS FILTER TO INITIAL ORBIT DETERMINATION OF A BREAK-UP," *Proceedings of the 6th European Conference on Space Debris*, 2013.

[6] M. P. W. Islam I. Hussein, Christopher W.T. Roscoe and J. Paul W. Schumacher, "Probabilistic Admissibility in Angles-Only Initial Orbit," *Proceedings of the 24th International Symposium on Space Flight Dynamics, Laurel, MD*, 2014.

[7] M. P. W. Islam I. Hussein, Christopher W.T. Roscoe and J. Paul W. Schumacher, "Probabilistic Admissible Region for Short-Arc Angles-Only Observations," *Proceedings of the Advanced Maui Optical and Space Surveillance Technologies Conference, Wailea, HI*, 2014.

[8] U. R. Mishra, S. Chakravorty, W. R. Faber, I. I. Hussein, S. G. Hesar, and B. Sunderland, "Geometric Solution to Probabilistic Admissible Region (PAR)," *The Journal of the Astronautical Sciences*, 2024.

[9] D. H. B. R. S. Mark Bolden, Dr. Islam Hussein and D. E. Griggs, "Probabilistic Initial Orbit Determination and Object Tracking in Cislunar Space Using Optical Sensors," *Proceedings of the Advanced Maui Optical and Space Surveillance Technologies Conference, Wailea, HI*, 2022.

[10] D. I. H. M. B. K. C. Dr. Erin Griggs, Matt Schierholtz and D. H. Borowski, "Probabilistic Initial Orbit Determination and Object Tracking in Cislunar Space Using Passive Radio Frequency Sensors," *Proceedings of the Advanced Maui Optical and Space Surveillance Technologies Conference, Wailea, HI*, 2023.

[11] M. Hejduk, "Specular and Diffuse Components in Spherical Satellite Photometric Modeling," *Proceedings of the Advanced Maui Optical and Space Surveillance Technologies Conference, Wailea, HI*, 2013.

[12] D. Raihan and S. Chakravorty, "Particle Gaussian mixture filters-I," *Automatica*, Vol. 98, 2018, pp. 331–340, https://doi.org/10.1016/j.automatica.2018.07.023.

[13] W. Faber, S. Chakravorty, and I. I. Hussein, "Multi-object tracking with multiple birth, death, and spawn scenarios using a randomized hypothesis generation technique (RFISST)," *2016 19th International Conference on Information Fusion (FUSION)*, 2016, pp. 154–161.

[14] I. I. H. W. F. S. H. B. S. Utkarsh R. Mishra, Suman Chakravorty, "Comparing Traditional and Admissible-Region Schemes For Angles-Only Initial Orbit," *Proceedings of the Advanced Maui Optical and Space Surveillance Technologies Conference, Wailea, HI*, 2023.

[15] I. Paranjape and S. Chakravorty, "CISLUNAR INITIAL ORBIT DETERMINATION AND TARGET TRACKING USING KINEMATIC FITTING AND PARTICLE GAUSSIAN MIXTURE FILTERING," preprint on webpage at `https://www.xcdsystem.com/aas/program/riGLvh6/index.cfm?pgid=5425`.

[16] R. Derbis, b. little, D. Meyer, and J. Hess, "ON ORBIT SENSING OF OBJECTS BEYOND GEO," 09 2022.

[17] H. Schaub and J. L. Junkins, *Analytical Mechanics of Space Systems*. Reston, VA: AIAA Education Series, October 2003, 10.2514/4.861550.

[18] J. Munkres, "Algorithms for the Assignment and Transportation Problems," *Journal of the Society for Industrial and Applied Mathematics*, Vol. 5, No. 1, 1957, pp. 32–38, 10.1137/0105003.

[19] D. L. Sara Bernardini, Maria Fox and J. Bookless, "Autonomous Search and Tracking via Temporal Planning," *Proceedings of the Twenty-Third International Conference on Automated Planning and Scheduling*, 2013.

[20] L. B. B. M. R. P. M. M. Ryan Whitley, Diane Davis and K. Howell, "EARTH-MOON NEAR RECTILINEAR HALO AND BUTTERFLY ORBITS FOR LUNAR SURFACE EXPLORATION," *Proceedings of the 2018 American Astronautical Society Astrodynamics Specialist Conference*, 2018.

[21] D. L. Sara Bernardini, Maria Fox and J. Bookless, "Multibody Orbit Architectures for Lunar South Pole Coverage," *Journal of Spacecraft and Rockets*, 2008.

[22] E. M. Z.-S. Stephen T. Scheuerle, Brian P. McCarthy and D. Davis, "RELATIVE MOTION FOR SHORT-TERM LOITERING IN THE GATEWAY NRHO," preprint on webpage at `https://www.xcdsystem.com/aas/program/riGLvh6/index.cfm?pgid=5425`.

[23] K. K. Boudad, *TRAJECTORY DESIGN BETWEEN CISLUNAR SPACE AND SUN-EARTH LIBRATION POINTS IN A FOUR-BODY MODEL*. Phd thesis, Purdue University, West Lafayette, IN, May 2021. Available at `https://engineering.purdue.edu/people/kathleen.howell.1/Publications/Dissertations/2022_Boudad.pdf`.